Combustion, gaseous emissions and PM characteristics of Di-Methyl Carbonate (DMC)-gasoline blend on Gasoline Direct Injection (GDI) engine

Chan, Jun; Tsolakis, Athanasios; Herreros, Martin; Kallis, Kyriakos; Hergueta Santos-Olmo, Cruz; Sittichompoo, Sak; Bogarra Macias, Maria

DOI:
10.1016/j.fuel.2019.116742

Document Version
Peer reviewed version

Citation for published version (Harvard):
Chan, J, Tsolakis, A, Herreros, M, Kallis, K, Hergueta Santos-Olmo, C, Sittichompoo, S & Bogarra Macias, M 2020, 'Combustion, gaseous emissions and PM characteristics of Di-Methyl Carbonate (DMC)-gasoline blend on Gasoline Direct Injection (GDI) engine', *Fuel*, vol. 263, 116742. https://doi.org/10.1016/j.fuel.2019.116742

Combustion, Gaseous Emissions and PM Characteristics of Di-Methyl Carbonate (DMC)-Gasoline Blend on Gasoline Direct Injection (GDI) Engine

J. H. Chan, A. Tsolakis*, J.M. Herreros, K. X. Kallis, C. Hergueta, S. Sittichompoo, M. Bogarra

Mechanical Engineering, University of Birmingham, B15 2TT, Birmingham, UK

*Email: a.tsolakis@bham.ac.uk

Abstract

The higher level of particle emissions of Gasoline Direct Injection (GDI) engines with respect to their counterpart port fuel injection engines motivated the introduction of legislative measures to limit their number in addition to the particulate matter (PM) mass. This study presents the impact on pollutant emissions of a potentially suitable oxygenated component, Di-Methyl Carbonate (DMC), as a supplement to gasoline fuel. Exhaust PM was characterised with Thermogravimetric Analysis (TGA) to understand its oxidation behaviour and composition, Transmission Electron Microscopy (TEM) to study the morphological characteristics of its agglomerate and Raman Spectroscopy (RAMAN) to analyse the particle nano-structure. Engine studied of an 8 % v/v DMC-gasoline fuel blend (D8) show similar combustion characteristics and fuel economy compared to gasoline. The combustion of DMC fuel blend reduced total unburnt hydrocarbon (THC) by approximately 30% and the number of PM emissions by 60%. Characterisation of particles formed by D8 demonstrated morphological and nano-structural alterations including a 10% reduction in primary particle size, leading to greater particles oxidation reactivity. The oxidation of particles emitted from the combustion of D8 started 15 °C earlier when compared to particles emitted from the gasoline combustion.

Keywords: GDI Engine, DMC, Gaseous Emissions, Particulate Matter, Nano-structure, Oxidation Reactivity

1. Introduction

In recent years, Gasoline Direct Injection (GDI) engine is being centred as the current trend in road transport vehicles because of its advantages of better power output, engine efficiency, and lower CO_2 emission when compared to conventional Port Fuel Injection (PFI) engine [**1, 2, 3**]. However, GDI engine has been reported to emit two to eight times greater concentration of particles in comparison to PFI engine [**3, 4, 5, 6**], this is due to piston and wall fuel impingement, local fuel rich regions and rich fuel droplets [**2, 7, 8**]. It has been reported that GDI engines emit similar or smaller size particle agglomerates than those emitted in compression ignition engines which can reach and reside in the lungs for longer period of time [**9, 10**]. Therefore, European Union has established a $6x10^{11}$ #/km limit in particulate matter (PM) emissions from GDI engines (Euro 6c) since September 2017.

One of the approaches to reduce particle emissions is the use of oxygenated fuels. Alcohols such as methanol, ethanol, and butanol are currently the most widespread alternatives. Ethanol could be produced from renewable feedstock being regarded as renewable and it can be used up to 85 % blended with gasoline [**11, 12**]. Other oxygenated such as MTBE (Methyl Ter-Butyl Ether) and ETBE (Ethyl Ter-Butyl Ether) are used to enhance octane number (i.e. allow the increase of compression ratio) and output power, and to promote cleaner fuel combustion [**13, 14, 15**]. However, MTBE and ETBE are non-renewable [**16, 17**] and MTBE could be hazardous to environment and human as potential carcinogen at high dosage [**14, 18**]. Di-Methyl Carbonate (DMC) can also be viewed as gasoline fuel substitute in spark ignition engines as it has low cost of production, non-reactive with metal (engine parts), non-toxic/irritant, good solubility with gasoline and can be produced from renewable sources [**12, 16, 17, 19, 20, 21**]. Recent studies revealed that DMC can be produced by using CO_2, however, low conversion rates and yield needs to be addressed [**22**]. DMC has been studied extensively on compression ignition engines as it improves carbonaceous exhaust emissions (including PM, unburnt hydrocarbons (HCs) and CO) [**23, 24, 25**] and engine thermal efficiency [**25, 26, 27**] mainly

due to its physiochemical properties, namely oxygen content (approximately 53.3 % m/m), kinematic viscosity (improves fuel injection spray) and low carbon to hydrogen (C/H) ratio. DMC has a molecular structure resulting in low tendency to form soot, thanks to the absence of C-C bonds and that one atom of oxygen is joined to two carbon atoms, thus oxygen can potentially inhibit soot formation from two carbon atoms [**28**]. Subsequently, DMC proved to suppress soot formation in kinetic modelling **[28]** and ethylene diffusion flame studies respectively [**29**]. Furthermore, particles produced from DMC addition to ethylene diffusion flames has been found to have higher soot oxidation reactivity than those formed from ethylene flames due to the variations found in the micro-structural and nano-structural particle characteristics [**29**].

There are limited studies on the use of DMC on spark ignition (SI) engines. DMC has illustrated positive effects on SI engine. DMC allowed to obtain higher indicate mean effective pressure (IMEP) under lean combustion ($\lambda = 1.1$) than ethanol and ETBE due to quicker flame speed of DMC has promoted the isochoric combustion [**30**]. Moreover, [**31**] concluded greater thermal efficiency with DMC blend in the view of better combustion enhanced by higher octane number and oxygen. Reductions on HC and CO emissions have been reported with DMC addition [**19, 31**] and oxygen content in DMC was identified to be the main reason through enhancing complete combustion. It has been reported that 5 % (v/v) of DMC addition is comparable to 10 % (v/v) of ethanol addition on the improvement of HC and CO emissions [**19**]. It is thought that the enhancement of complete combustion and the low heating value (LHV) of DMC result in higher CO_2 emissions compare to gasoline and other oxygenates such as ethanol and ETBE [**30**]. There is no agreement regarding the effect of DMC on NO_x with respect to gasoline. For instance, NOx reductions were found in [**19**] when lambda was close to 1, while non-significant effects in NO_x were found for non-stoichiometric engine operation. NOx reductions at stoichiometric engine operation were justified by a reduction in the flame temperature by DMC addition. However, work [**31**] has also reported higher NOx emissions with DMC, as a result of the

higher in-cylinder combustion temperature. Whereas, DMC was found to have non-observable effect under stoichiometric and lean mixtures in a kinetic modelling study by [**28**] due to the absence of ketenyl radicals (HCCO).

Previous studies agreed on the reduction of un-burnt hydrocarbons, carbon monoxide and particle emissions when DMC is added to gasoline fuel in GDI engines, while there are some discrepancies on the effect on NOx emissions. However, there is no comprehensive investigation on the effect of DMC-gasoline blends on particle emissions characteristics such as morphology, nano-structure from GDI engines. Therefore, this investigation studies the effect of DMC-gasoline blend on gaseous and particle emissions with main focus on particle reactivity through particle size, morphology and nano-structure characterisation. Results of this work assess the feasibility of DMC as alternative fuel in GDI engines as well as provide guidelines to understand its potential impact on human and environment.

2. Experimental Setup and Methodology

2.1 Engine Test Bench

Table 1: Engine Specification

A four-cylinder turbocharged 2 L engine was used to conduct the experiments in a test rig as illustrated in the simplified schematic in **Figure 1**. The engine is equipped with air-guided side-mounted solenoid direct fuel injectors with the spark plugs centrally positioned on top of each of the four cylinders. Further engine specifications are presented in **Table 1**. A 75kW AC dynamometer and inverter drive is coupled to the engine. The dynamometer is controlled with CADET control system supplied by CP

Engineering. Fuel consumption was recorded from Rheonik RM 015 with fuel-conditioning unit to maintain the fuel temperature at 28 ˚C. An AVL miniature piezo-electric pressure transducer Baumer 720 was utilized for in-cylinder monitoring. Two National Instrument cards were used for high and low speed data acquisition (DAQ) in LabView software and post-processed in Matlab using an in-house developed script for detailed combustion analysis inclusive of mass fraction burned (MFB), coefficient of variation (COV) of IMEP and maximum in-cylinder pressure (P_{max}). Each in-cylinder pressure profile is obtained by an average of 200 consecutive cycles. The first law of thermodynamics has been applied to calculate net rate of heat release. Particularly, the equation shown below was used to estimate the net heat release rate. In-cylinder pressure data is experimentally measured while the ratio of specific heats (γ) for the cylinder contents was estimated from the gradient of the logarithmic pressure-volume curve during the compression and expansion phases, and smoothed at the transition.

$$\frac{dQ}{d\theta} = \frac{\gamma}{\gamma - 1} p \frac{dV}{d\theta} + \frac{1}{\gamma - 1} V \frac{dp}{d\theta} \qquad \textit{Equation 1}$$

The normalised mass fraction of fuel burned curve (Figure 3) is the ratio of the cumulative/integral heat release, QR_{Cum} to the total heat release, QR_T following the equation below.

$$MFB_{(\theta)} = \frac{QR_{cum\,(\theta)}}{QR_T} \qquad \textit{Equation 2}$$

An interface software provided by Accurate Technologies Inc. manages electronic control unit (ECU), which enabled the variable of spark timing, fuel injection parameters and intake/exhaust valves phasing. Sensor readings and other calculated parameters can be simultaneously obtained with DAQ collection through controller area network (CAN). The engine is configured to a default calibration strategy to reduce pumping losses by valve overlapping (internal exhaust gas recirculation) to increase the residuals exhaust gas. The engine is equipped with a commercial Three-Way Catalyst (TWC).

Figure 1: Schematic Drawing of Experimental Setup

2.2 Gaseous and Particle Size Analysers

Gaseous emissions (Total hydrocarbons (THC), CO, CO_2 and NOx) were analysed with MKS FTIR (Fourier transform infrared) analyser through a conditioning unit in order to avoid damage on the optical lenses by the PM. The FTIR has a 10-100 ppb sensitivity to measure exhaust components. The lowest detectable limits are 1.2 ppm, <1 ppm and 3.6 ppm for CO, HC species and NOx, respectively. TSI SMPS (scanning mobility particle sizer) composed of 3081 DMA (differential mobility analyser), 3080 electrostatic classifier and 3775 CPC (condensation particle counter) was used to measure the particle concentration to obtain particle size distribution (PSD). The CPC that forms part of the SMPS system has a particle count accuracy of ± 10% for particle concentrations lower than $5x10^4$ particles/cm^3 and ± 20% for particle concentrations lower than 107 particles/cm^3. A one-stage temperature-controlled ejector dilution system was used at dilution ratio (α) of 10. Dilution ratio is constantly monitored using NO and CO_2 as Eq.1 shows. The dilutor was controlled at 200°C and supplied with heated air at 150 °C. A high efficiency particle arrestance (HEPA) filter was installed prior the dilution air inlet. The sample sheath and sample flow rates in the SMPS were set at 10.00 and 1.00 litres per minute respectively to obtain PSD ranged between 7.77 to 294 nm. The sampling points for FTIR and SMPS are before Three-Way Catalyst (bTWC) indicated in **Figure 1**. Heated lines were maintained to 191 °C as preventive measure to avoid condensation of HCs and water during the exhaust gases transportation to the instruments.

$$\alpha = \frac{CO_{2_{diluter\ inlet}}}{CO_{2_{diluter\ outlet}}} \text{ x } 100\ \% \qquad \textbf{(Eq. 1)}$$

2.3 Oxidation Activity and Nano-structural Analysis

LLG GF/F Glass microfiber filters, with a diameter of 47 mm were used for PM loading with filter holder via pump extraction from exhaust system. PM loaded filters were utilized for Perkin Elmer Thermogravimetric analyser, Pyris 1 to evaluate the oxidation activity. PM Loaded filters were also used for Renishaw Raman Spectroscopy (RAMAN), inVia to conduct nano-structural analysis on PM.

2.4 Grids

TAAB 3.05mm Formvar-Carbon copper grids were used to obtain PM agglomerates by direct exposure to the exhaust tailpipe. Subsequently the agglomerate images were captured with JEOL 2100 transmission electron microscope (TEM) at 200keV for primary particles and morphological analysis.

2.5 Test Fuels

Commercial gasoline, EN 228 provided by Shell containing 10 (v/v %) of ethanol was used in this experimental study as baseline fuel. DMC was purchased from Alfa Aesar UK, with purity (GC) of equivalent or more than 98.5 %. DMC-gasoline blending was denoted as D8 to indicate the percentage of DMC blend of 8 (v/v %) and was splash blended with commercial gasoline. Properties of fuels are listed in **Table 2**. Integrity test on the blend was carried out to ensure no phase separation occurred with gasoline by storing it for two weeks under room temperature.

Table 2: Fuels Properties

2.6 Experimental Procedures

The experimental tests were carried out at 2200 rpm/90 Nm corresponding to a condition from light duty New European Driving Cycle (NEDC) for vehicles. Engine stoichiometry and homogeneity were maintained throughout the test. Please find further details of the engine settings in **Table 3**. Engine was warmed up to 90 $\pm$ 0.5 ˚C and 95 $\pm$ 2 ˚C for engine coolant and oil temperatures respectively to ensure high engine stability prior to test begins. Internal EGR (exhaust gas recirculation) was removed by setting IVO (intake valves opening) and EVC (exhaust valves closing) to 11 aTDC (Top Dead Centre) and 8 aTDC to enhance combustion stability and avoid its influence on gaseous and particle emission characteristics**.**

Table 3: Experimental Matrix of Engine Bench Test

Gaseous emissions were measured with an MKS FTIR gas analyser for at least 300 seconds and PSD was averaged with 5 measurements to ensure its repeatability and reliability. Microfiber glass filters were placed in furnace at 500 ˚C for 5 hours to prevent any material loss and to remove aromatics as pre-treatment. Filter holder was kept approximately at 200 ˚C with external heating and insulated during loading process (30 minutes for gasoline and 45 minutes for D8).

2.7 Particle Composition and Reactivity

Figure 2: TGA Temperature Ramp Program

Table 4: TGA Methodology

A cylindrical hollow pipe was used to cut the PM loaded filters into discs with a suitable size for thermogravimetric (TGA) and RAMAN analysis. TGA procedure as shown in **Table 4** (heating ramps at 3 ˚C/min) enables to estimate maximum mass lost rate temperature (MMLRT), PM composition and soot oxidation mass profile. The balance of the TGA has an accuracy better than 0.02%, sensitivity of 0.1 µg and reproducibility to ± 2µg. The furnace has a temperature precision of ± 2°C. PM emissions are distinguished into two different nature, the Volatile Organic Materials (VOMs) and elemental soot. VOMs are formed by THCs adsorbed on the soot surface derived from the fuel and lubricant. Step 1 to 4 are the volatilisation phase to remove VOMs and water on the filter to prevent the inference of soot oxidation reactivity (see **Figure 2**). Meanwhile step 5 to 8 are the oxidation phase to evaluate the soot reactivity of particles emitted from both fuels. Two different tests were performed on the thermogravimetric analyser to obtain i) PM composition and ii) soot oxidation mass profile. Tests were completed by analysing the same mass of PM for gasoline and D8 (summation of VOMs and soot) to ensure fair comparison while acquiring soot oxidation mass profile and MMLRT to avoid inaccurate data acquired due to mass effect as previously reported [**32**].

2.8 Particle Nano-structure

Four PM samples were used in the RAMAN analysis. Laser intensity was set at 1 % to prevent burning of PM sample on filter under 100x magnification. Spectra were obtained with 10 accumulations. Each accumulation was obtained with laser exposure time of 30 seconds. Results were post-treated with specialised software, Renishaw WiRE for deconvolution (curves fitting) and data acquisition using the combination of 3 Lorentzian and 1 Gaussian (3G1L). Methodology of 3L (band G ~ 1590 cm^{-1}, D_1 ~ 1360 cm^{-1}, and D_4 ~ 1180 cm^{-1}) and 1G (band D_3 ~ 1500 cm^{-1}) was evaluated to provide closest correlation

and consistency to soot oxidation reactivity with lowest fitting error, $\chi 2$. Furthermore, this method is able to estimate similar fringe length to the values measured from TEM analysis [**33**].

2.9 Particle Morphology

Primary particle size (dp_0) evaluation was performed with the use of a MATLAB built digital image software. Measurements were carried for at least 450 primary particles found in 25 agglomerates for each fuel. Particle measurements were completed only on identifiable particle boundaries, to ensure good accuracy of estimation which is crucial for the morphological analysis. A representative number of primary particles from TEM grids have been analysed performing log-normality check test on IBM statistical package for social sciences (SPSS). This will limit the influence of subjectivity in recognizing particles boundaries in the precision of diameter dimensions [**34, 35**]. TEM images were pre-treated to remove background and contrast adjustment to aid in primary particle recognition. It was later post-processed with an in-house MATLAB script to determine the number of primary particles (n), radius of gyration (R_g) and fractal dimension (D_f) which was previously used by [**34**] for a comparison study on five D_f methodologies. A comparison was made with Root Form Factor (RFF) and logarithm method using R_g (Power Law Relationship method) and square root of production length and width (Minimum Bounding Rectangle method). Hence, the MATLAB script was developed by referring Eq.2 to Eq. 6. RFF is a non-dimensional parameter and is the ratio of area to perimeter, which is comparable to D_f. Meanwhile, D_f using Power Law Relationship and Minimum Bounding Rectangle methods were obtained with evaluating the gradient of linear regression line.

$$n = \left(\frac{A}{A_p}\right)^a \qquad \textbf{(Eq. 2)}$$

Where, n is the number of primary particles per agglomerate, A is area of agglomerate as projected in the micrograph, A_p is area of the primary particle considered as a circle using formula $A_p = (\pi/4)d_{p0}^2$, a is exponential factor for particle overlap, assumed to be 1.09 [**36**].

$$R_g = \sqrt{\frac{1}{m}\sum r_i^2} \qquad \textbf{(Eq. 3)}$$

Where, R_g is the radius of gyration, m is the number of pixels per agglomerate, r_i is the distance between the centre of a primary particle and the centroid of the agglomerate.

(Minimum Bounding Rectangle Method)

$$\ln n = \ln k_f + D_f \ln\left(\frac{\sqrt{LW}}{dp_0}\right) \qquad \textbf{(Eq. 4)}$$

(Power Law Relationship Method)

$$\ln n = \ln k_f + D_f \ln\left(\frac{R_g}{dp_0}\right) \qquad \textbf{(Eq. 5)}$$

(Root Form Factor)

$$RFF = \sqrt{\frac{4\pi A_p}{Perimeter^2}} \qquad \textbf{(Eq. 6)}$$

Where, k_f is the pre-factor or structural coefficient [**37**], L and W are the length and width respectively of rectangle containing the minimum area, d_{p0} is the primary particle size (nm).

3. Results and Discussion

3.1 Combustion Analysis

Mass Fraction Burnt (MFB) is shown in **Figure 3.** MFB50 of D8 blend combustion was phased by slightly varying spark timing to obtain same combustion profile to baseline gasoline for Maximum Brake Torque (MBT) condition. **Figure 4** shows the results of brake specific fuel consumption (BSFC), brake thermal efficiency (BTE) and exhaust gas temperature for D8 and gasoline combustion. BSFC of D8 blend is approximately 10 % higher compared to the BSFC obtained from gasoline fuel. BTE is calculated in order to compare fuel economy considering the lower heating value of the D8 blend with respect to gasoline. BTE for both fuels are the same (changes lesser than 1 %) which indicates that the increase in fuel consumption (BSFC) for D8 fuel blend its entirely due to the lower energy density of DMC in comparisons to gasoline. Exhaust temperature for case of D8 was lower than gasoline. It is thought that the lower exhaust gas temperature reflects a lower in-cylinder temperature due to the high heat of vaporisation of DMC cooling down the combustion chamber [**38**]. The combustion stability of D8 was maintained with respect to gasoline as illustrated by negligible difference in COV_{IMEP} values (see **Figure 5**), being all of them below the recommended value of 5 % to assure stable combustion [**1**]. Therefore, the maximum in-cylinder pressure (P_{Max} in-cylinder) was not affected and displayed similar values for both gasoline and D8 at 40.9 and 40.7 bar, respectively.

Figure 3: MFB plot for Gasoline and D8.

Figure 4: Exhaust Gas Temperature, Brake Thermal Efficiency and Equivalent Brake Specific Fuel Consumption

Figure 5: Maximum In-Cylinder Pressure and COV of IMEP

3.2 Gaseous Emissions

THC emitted by D8 show a statistically significant reduction of 30 % with respect to gasoline combustion. This is the result of reductions in each of the hydrocarbon species measured with the exception of toluene (**Figure 6a** and **6b**). However, D8 result in a slight increase in CO and CO_2 emissions (by 7 % and 4 %, respectively) compare to gasoline combustion. It has to be noted that the difference in CO emissions is not statistically significant as the confidence intervals are overlapped. The trade-off between THC and CO is attributed to the oxygen in DMC which had facilitated the post-combustion oxidation of some hydrocarbon species [**39, 40**] being partially oxidised to CO. Additionally, greater BSFC with DMC addition had led to more CO_2 formation despite the lower carbon content in D8 blend with respect to gasoline.

Figure 6: (a) Specific gaseous **(b)** HC species emissions for gasoline and D8

In regard to NO_x emissions, there is not a statistically significant difference (lesser than 1 %) between D8 and gasoline combustion. Generally, NO_x was claimed to form via Zeldovich mechanism, also known as thermal NO_x by relating the combustion temperature to NO_x formation (mainly nitric oxide, NO) [**41, 42**]. Potential NO_x reductions for D8 were predicted as a result of lower in-cylinder temperature and presence of HCCO radicals from during the DMC combustion, which could react with the formed NO. However, it is thought that the presence of oxygen in DMC has attacked the HCCO

radicals, thus HCCO-NO reaction did not take place and NO_x remained similar concentration to gasoline [**28, 43**].

3.3 Particulate Matter

3.3.1 Particle Size Distributions and Composition

Unimodal PSDs were obtained from the combustion of both gasoline and D8 fuels (**Figure 7a**). Geometry number mean diameter (GNMD) was reduced from 46 nm to 41 nm and total particle number concentration was decreased by about 60 % when D8 was used compared to gasoline combustion. The decline of GDNM was not due to greater number of smaller particles but rather due to a reduction in large particles. This is further affirmed by the mass PSD presented in **Figure 7b** [**44**]. It is believed that the lower particle concentration with D8 reduced the number of particles to particle interactions (e.g. coagulation, agglomeration, aggregation) leading to smaller agglomerates [**1, 44**]. The main reasons to justify such reduction in particle concentration and size is the presence of oxygen in DMC, higher oxygen/carbon (O/C) ratio [**45**], lower C/H ratio, absence of C-C bonds and absence of aromatic compounds [**46**] which hinder soot formation and growth rates and promote soot oxidation during the combustion process. The ability of DMC to suppress soot precursors such as C2 hydrocarbons (acetylene) is shown in **Figure 6b** and reported in other works [**28, 47**] which also contribute to reduction in soot formation and particle growth rate. **Figure 7** also shown the majority of particle reductions are within the size range attributed to solid soot particles (accumulation mode) [**32**]. In addition, PM composition analysis (see **Figure 8**) presents ratio of VOMs to elemental soot. A Higher percentage of volatile organic material (e.g. unburned fuel and/oil derived hydrocarbons, water and other fuel and lubricant components) in D8 particles compared to particles emitted from gasoline combustion is obtained. This result further supports the hypothesis that reduction in particles is due to a considerable reduction in soot content.

Figure 7: Particle Size Distribution by **(a)** Number **(b)** Mass emitted by gasoline and D8

Figure 8: PM Compositions for gasoline and D8

3.3.2 Particle Reactivity

Combustion of oxygenated fuels tend to form soot with high oxidation reactivity in both GDI and compression ignition engines [**48, 49, 50**]. D8 soot is more reactive by displaying the start of oxidation temperatures for D8 and gasoline at approximately 300 ˚C and 315 ˚C, respectively (**Figure 9a**). It is also further supported by the sharper and earlier MMLRT peak (**Figure 9b**) towards about 495 ˚C compared to gasoline at 510 ˚C. The higher VOMs to elemental soot ratio of D8 particles with respect to gasoline fuel particles was believed to be one of the reasons. The prime aim of devolatilisation stage in TGA is to remove VOMs to prevent interferences with soot oxidation results. However, this stage has been reported to increase the porosity of particles being more vulnerable to oxygen penetration which in turn, leads to higher soot oxidation rate [**50**]. Thus, particles formed with D8 blend are related to more rapid oxidation activity. There are also other root-causes attributed in the literature to affect the oxidation reactivity including primary particle size and nano-structure of particles [**48, 49**]. Therefore, this study was extended to TEM (primary particle size and particle morphology) and RAMAN analysis (particle nano-structure) to further evaluate the reasoning for the reactivity difference between the two fuels.

Figure 9: (a) Soot Oxidation Mass Profile **(b)** Maximum Mass Loss Rate Temperature for soot emitted by gasoline and D8

3.3.3 Particle Morphology

Figure 10: TEM Micrographs of PM agglomerate for gasoline (*left*) and D8 (*right*) at 80k magnification

PM agglomerates are in form of aciniform-shape made up of multiple primary particles as shown in **Figure 10**. In general, large agglomerates, diesel-like particles and particles in clusters or chain formations were identified from all of the TEM micrographs analysed in this work as suggested in literature [**34, 51**]. The primary particle size obtained from the TEM micrographs behaves like a log-normal size distribution with a wide size range from 5 to 70 nm. Primary particles measured have satisfied the IBM SPSS log-normality one-sample Kolmogorov-Smirnov test performed as shown in **Table 5, Figure 11a** and **11b**. Average primary particle dimeter (dp_0) is obtained from the distributions (see **Figure 11c**) indicating D8 combustion tends to form smaller primary particles (average 22.53 nm) compared to primary particles emitted from gasoline combustion (average 25.40 nm). The smaller primary particle is explained by the presence of oxygen, lower C/H ratio, and reduced aromatics with DMC addition. These are thought that oxygen restricts the particle surface growth by simultaneously suppressing the soot formation rate and promoting soot oxidation during combustion [**45**]. Secondly, the reduction on number of solid soot particles (larger primary particles) due to absence of C-C bond of D8 blend is also a key reason. Consequently, it reduced the average number of particles per agglomerate (**Figure 12a**) and as subsequent effect, it had led to smaller aggregate particle size, consistent to the SMPS results previously showed. A decline in the formation of primary particles have led to the R_g to decrease from 95 to 77 nm which is consistent to the trend shown in PSD obtained with the SMPS (**Figure 7**) and similar to results reported in the literature [**34**]. Higher soot reactivity was reported to be linked to the smaller primary particles as it increases the specific surface area, SSA (surface area/volume) ratio. Higher SSA means more surface area available for oxygen contact during

oxygen [**49, 50**]. Thus, the improvement of soot oxidation explained in previous section is thought that is partially due to the influence of smaller primary particles formation by D8.

Table 5: Statistical Normality Tests

Figure 11: Primary Particle Distribution for **(a)** gasoline (G), **(b)** D8 and **(c)** Average Primary Particle Size

Figure 12: (a) Number of Primary Particles per Agglomerate and Radius of Gyration **(b)** Fractal Dimension

Fractal dimension (D_f) determines the geometrical morphology of primary particle by the evaluation of compactness of primary particles in the agglomerates [**34, 50**] as well as to predict the type of collisions occurred [**52**]. Higher compactness (higher D_f) represents cluster geometry agglomerate, while lower D_f means more chain-like agglomerate [**53**]. Three different methodologies were used to calculate D_f to ensure the consistency of the results obtained. All values obtained from all methodologies demonstrated a consistent trend showing a majority of gasoline agglomerates are less compact than D8 agglomerates (lower D_f values). Therefore, D8 agglomerates are less chain-like with respect to gasoline. Chain-like agglomerates are caused by collisions of primary particles and smaller agglomerate [**54**]. Agglomerates from the combustion of D8 fuel was found to have higher D_f (**Figure 12b**) that can be explained by smaller number of collisions taking place as a result of the lower number of primary particles, np_0. The results also indicate DMC addition modified the collision mechanisms between primary particles and agglomerates in comparison to gasoline due to the variation of mean

free path [**55**]. Lower R_g and agglomerate concentration (PSD in **Figure 7**) in the case of D8 had promoted greater mean free path and therefore leading to the 'ballistic' collision subsequently less chain-like agglomerates via cluster-cluster agglomeration. Conversely for gasoline, it was dominated by 'diffusion limited' mechanism because of the lesser mean free path available with higher R_g and agglomerate concentrations by the tip of agglomerates. It was pointed out [**56**] that higher surface area was connected to lower D_f, due to its chain-like geometry, promoting soot oxidation. However, particles emitted from D8 combustion showed a higher soot reactivity not through its higher fractal dimension.

3.3.4 Particle Nano-structure

Figure 13: Average Raman Spectra

Table 6: I_{D1}/I_G, A_{D1}/A_G, I_{D3}/I_G, A_{D3}/A_G and L_a obtained from Raman spectra for gasoline and D8.

$$L_a = 4.4 \left(\frac{A_{D1}}{A_G}\right)^{-1} \qquad \textbf{(Eq. 7)}$$

Where, L_a is the fringe length and $\frac{A_{D1}}{A_G}$ is the ratio area of band D1 to band G.

RAMAN is an analytic tool with capability of providing chemical and structural information of particles through its fingerprint spectra [**57**]. An average of 10 Raman spectra were obtained from soot samples derived from the combustion of gasoline and D8 (**Figure 13**). The spectra were de-convoluted and the values of I_{D1}/I_G (ratio intensity of band D1 to band G), A_{D1}/A_G, D1 FWMH (width at half maximum of band D1), I_{D3}/I_G (ratio intensity of band D3 to band G) and A_{D3}/A_G (ratio area of band D3 to band G) are

calculated and tabulated in **Table 6**. Soot primary particles are formed by two main parts (inner core and outer shell). Inner core may contain up to several individual nuclei built up by random and highly disorder arranged graphene layers (amorphous content) [**4**]. These nuclei are the result of rapid soot formation and coalescence of particles during particles growth process. While the outer shell composed of structured graphene layers with some amorphous portion was found within the shell [**58**]. Intensity ratio and area ratio of D_1 to G (I_{D1}/I_G and A_{D1}/A_G), and D1 FWMH were used to evaluate the magnitude of disorder of graphene layer edges, while intensity ratio and area ratio of D_3 to G (I_{D3}/I_G and A_{D3}/A_G) are for identifying amorphous soot concentration in PM which composed of organic molecules, fragments and functional groups [**33**]. Regarding D8, graphene layer edges was found to be smaller in graphitic order of magnitude (greater band D1) and higher in amorphous (greater band D3) concentration. Soot primary particle formation is initiated with amorphous graphene layer, it crystallised under the exposure of heat towards the nucleus from the outer shell. The reason is because of the lower in-cylinder temperature running on D8 blend reduces the graphitization process of graphene layers. Hence fewer crystalline structured soot was formed as result of lower fraction of amorphous graphene have undergone graphitization process under lower in-cylinder temperature with D8 blend [**49**]. Active sites on surface available for oxidation were enlarged due to the higher disorder (amorphous) which led to higher soot reactivity as shown in TGA (see **Figure 9a** and **9b**) [**59**]. Higher amorphous concentration is linked to wider distribution and higher mean value of fringe tortuosity, F_t [**60**]. According to *Serhan et al* [**50**], F_t has major effect on soot oxidation. The latter was attributed to the weaker C-C bonds (breakdown easily) due to the effect of strain imposed on the bond which causes atomic orbitals overlap and lowered the resonance stabilization.

The modified Knight and White's formula (**Eq. 7**) by *Seong et* al had proven the combination of 3L1G fittings had given similar estimation of fringe length (L_a) values to TEM image analysis [**33**]. Results of L_a and I_{D1}/I_G are presented in **Table 6** showing a longer L_a for gasoline with respect to D8. L_a is associated

to graphene layer length and serves an indication to number of carbon on edge site [**60**]. Lower L_a indicates higher number of carbons located on the edge site, which was associated to higher reactivity. Consequently, formation of bond with chemisorbed oxygen is much easier compared to basal plane atom with greater accessibility of oxygen [**61, 62**]. Thus, in this study D8 shows to possess higher number of carbons located on the edge site, it is believed be another contributing factor to enhance soot reactivity [**50**].

4. Conclusions

The effect of 8 % (v/v) DMC blended with EN228 commercial gasoline was evaluated on engine performance and exhaust emissions with a four-cylinder GDI turbocharged engine. Particulate matter characteristics including particle oxidation reactivity, primary particle size, morphology, and nano-structure were for first time comprehensively investigated.

This investigation of a DMC-gasoline fuel blend has demonstrated a reduction of 30% in unburnt hydrocarbon species and of 60% in total number of PM emissions, while there are no significant differences in the combustion patterns and brake thermal efficiency with respect to conventional gasoline engine fuelling. D8 significantly reduced It is understood that the fuel oxygen content of DMC and its advantageous chemical structure are the main responsible of such reductions.

The smaller primary particle diameter (higher surface area for oxidation), greater amorphous carbon content (weaker C-C bonds) and shorter fringe length (more active sites for particles oxidation) from particles emitted from D8 combustion results in a lower onset temperature for particle oxidation (15°C) and higher particle oxidation reactivity compare to particles emitted from gasoline combustion. The higher reactivity can benefit the gasoline particulate filters (GPFs) regeneration strategies by reducing energy required and frequency of regeneration events to oxidise accumulated particles. This

will reduce the fuel penalty associated to active regeneration of particulate filters. Meanwhile lesser PM concentration and smaller agglomerates (lower radius of gyration) emitted by D8 combustion could reduce the back pressure induced on the GPFs and subsequently minimising the drop of fuel economy as resultant of pressure drop.

Therefore, it presents DMC as a potential candidate for GDI engines to achieve the emissions limits and to reduce harmful emissions to human and the environment. Effects of DMC can be further assessed on the TWC and GPF in future to ensure applicability on vehicle to meet current and future legislations.

Acknowledgements

Jun Hoe Chan would like to thank University of Birmingham for his scholarship. ESPRC is acknowledged for supporting this work with the project “FACE” (ESPRC: ref. EP/P03117X/1).

References

[1] M. Bogarra, J. M. Herreros, A. Tsolakis, A. P. E. York, and P. J. Millington, "Study of particulate matter and gaseous emissions in gasoline direct injection engine using on-board exhaust gas fuel reforming," *Applied Energy,* vol. 180, pp. 245-255, 2016.

[2] C. L. Myung and S. Park, "Exhaust nanoparticle emissions from internal combustion engines: A review," *International Journal of Automotive Technology,* vol. 13, no. 1, pp. 9-22, 2012.

[3] R. C. Zhu, J. N. Hu, X. F. Bao, L. Q. He, Y. T. Lai, L. Zu, Y. F. Li, and S. Su, "Tailpipe emissions from gasoline direct injection (GDI) and port fuel injection (PFI) vehicles at both low and high ambient temperatures," *Environmental Pollution,* vol. 216, pp. 223-234, 2016.

[4] A. Liati, D. Schreiber, P. D. Eggenschwiler, Y. A. R. Dasilva, and A. C. Spiteri, "Electron microscopic characterization of soot particulate matter emitted by modern direct injection gasoline engines," *Combustion and Flame,* vol. 166, pp. 307-315, 2016.

[5] C. L. Reddington, K. S. Carslaw, D. V. Spracklen, M. G. Frontoso, L. Collins, J. Merikanto, A. Minikin, T. Hamburger, H. Coe, M. Kulmala, P. Aalto, H. Flentje, C. Plass-Duelmer, W. Birmili, A. Wiedensohler, B. Wehner, T. Tuch, A. Sonntag, C. D. O'Dowd, S. G. Jennings, R. Dupuy, U. Baltensperger, E. Weingartner, H. C. Hansson, P. Tunved, P. Laj, K. Sellegri, J. Boulon, J. P. Putaud, C. Gruening, E. Swietlicki, P. Roldin, J. S. Henzing, M. Moerman, N. Mihalopoulos, G. Kouvarakis, V. Zdimal, N. Zikova, A. Marinoni, P. Bonasoni, and R. Duchi, "Primary versus secondary contributions to particle number concentrations in the European boundary layer," *Atmospheric Chemistry and Physics,* vol. 11, no. 23, pp. 12007-12036, 2011.

[6] R. Niessner, "The many faces of soot: characterization of soot nanoparticles produced by engines," *Angew Chem Int Ed Engl,* vol. 53, no. 46, pp. 12366-79, 2014.

[7] M. A. Attar and H. M. Xu, "Correlations between particulate matter emissions and gasoline direct injection spray characteristics," *Journal of Aerosol Science,* vol. 102, pp. 128-141, 2016.

[8] M. M. Maricq, D. H. Podsiadlik, D. D. Brehob, and M. Haghgooie, "Particulate Emissions from a Direct-Injection Spark-Ignition (DISI) Engine," *SAE Technical Paper 1999-01-1530,* 1999.

[9] K. Donaldson, X. Y. Li, and W. MacNee, "Ultrafine (nanometre) particle mediated lung injury," *Journal of Aerosol Science,* vol. 29, no. 5-6, pp. 553-560, 1998.

[10] M. Riedl and D. Diaz-Sanchez, "Biology of diesel exhaust effects on respiratory function," *J Allergy Clin Immunol,* vol. 115, no. 2, pp. 221-8; quiz 229, 2005.

[11] H. Jafari, M. H. Idris, A. Ourdjini, H. Rahimi, and B. Ghobadian, "Effect of ethanol as gasoline additive on vehicle fuel delivery system corrosion," *Materials and Corrosion-Werkstoffe Und Korrosion,* vol. 61, no. 5, pp. 432-440, 2010.

[12] C. L. Peng, K. C. Lewis, and F. P. Stein, "Water solubilities in blends of gasoline and oxygenates," *Fluid Phase Equilibria,* vol. 116, no. 1-2, pp. 437-444, 1996.

[13] R. Cataluña, D. Dalávia, R. da Silva, E. Menezes, V. Venturi, and R. Wagner, "Acceleration tests using gasolines formulated with di-TAE, TAEE and MTBE ethers," *Fuel,* vol. 90, no. 3, pp. 992-996, 2011.

[14] F. Nadim, P. Zack, G. E. Hoag, and S. L. Liu, "United States experience with gasoline additives," *Energy Policy,* vol. 29, no. 1, pp. 1-5, 2001.

[15] R.-H. Chen, L.-B. Chiang, C.-N. Chen, and T.-H. Lin, "Cold-start emissions of an SI engine using ethanol–gasoline blended fuel," *Applied Thermal Engineering,* vol. 31, no. 8-9, pp. 1463-1467, 2011.

[16] A. Arteconi, A. Mazzarini, and G. Di Nicola, "Emissions from Ethers and Organic Carbonate Fuel Additives: A Review," *Water Air and Soil Pollution,* vol. 221, no. 1-4, pp. 405-423, 2011.

[17] R. R. Ginting, A. Mustain, and G. Wibawa, "Determination of Ternary Liquid–Liquid Equilibria for Dimethyl Carbonate + 2-Methyl-1-propanol or 2-Methyl-2-propanol + Water Systems at T = 303.15 and 313.15 K," *Journal of Chemical & Engineering Data,* vol. 62, no. 1, pp. 463-468, 2017.

[18] F. Belpoggi, M. Soffritti, and C. Maltoni, "Methyl-tertiary-butyl ether (MTBE)--a gasoline additive--causes testicular and lymphohaematopoietic cancers in rats," *Toxicol Ind Health,* vol. 11, no. 2, pp. 119-49, 1995.

[19] L.-b. Wen, C.-Y. Xin, and S.-C. Yang, "The effect of adding dimethyl carbonate (DMC) and ethanol to unleaded gasoline on exhaust emission," *Applied Energy,* vol. 87, no. 1, pp. 115-121, 2010.

[20] P. Tundo, "New developments in dimethyl carbonate chemistry," *Pure and Applied Chemistry,* vol. 73, no. 7, pp. 1117-1124, 2001.

[21] M. A. Pacheco and C. L. Marshall, "Review of Dimethyl Carbonate (DMC) Manufacture and Its Characteristics as a Fuel Additive," *Energy & Fuels,* vol. 11, no. 1, pp. 2-29, 1997.

[22] P. Kongpanna, V. Pavarajarn, R. Gani, and S. Assabumrungrat, "Techno-economic evaluation of different CO2-based processes for dimethyl carbonate production," *Chemical Engineering Research and Design,* vol. 93, pp. 496-510, 2015.

[23] P. Rounce, A. Tsolakis, P. Leung, and A. P. E. York, "A Comparison of Diesel and Biodiesel Emissions Using Dimethyl Carbonate as an Oxygenated Additive," *Energy & Fuels,* vol. 24, pp. 4812-4819, 2010.

[24] C. S. Cheung, R. Zhu, and Z. Huang, "Investigation on the gaseous and particulate emissions of a compression ignition engine fueled with diesel-dimethyl carbonate blends," *Sci Total Environ,* vol. 409, no. 3, pp. 523-9, 2011.

[25] Z. H. Huang, D. M. Jiang, K. Zeng, B. Liu, and Z. L. Yang, "Combustion characteristics and heat release analysis of a direct injection compression ignition engine fuelled with diesel-dimethyl carbonate blends," *Proceedings of the Institution of Mechanical Engineers Part D-Journal of Automobile Engineering,* vol. 217, no. D7, pp. 595-605, 2003.

[26] D. Q. Mei, S. Yue, X. D. Zhao, K. Hielscher, and R. Baar, "Effects of center of heat release on combustion and emissions in a PCCI diesel engine fuelled by DMC-diesel blend," *Applied Thermal Engineering,* vol. 114, pp. 969-976, 2017.

[27] G. D. Zhang, H. Liu, X. X. Xia, W. G. Zhang, and J. H. Fang, "Effects of dimethyl carbonate fuel additive on diesel engine performances," *Proceedings of the Institution of Mechanical Engineers Part D-Journal of Automobile Engineering,* vol. 219, no. D7, pp. 897-903, 2005.

[28] M. U. Alzueta, P. Salinas, Á. Millera, R. Bilbao, and M. Abián, "A study of dimethyl carbonate conversion and its impact to minimize soot and NO emissions," *Proceedings of the Combustion Institute,* vol. 36, no. 3, pp. 3985-3993, 2017.

[29] C. Paladpokkrong, D. Liu, Y. Ying, W. Wang, and R. Zhang, "Soot reduction by addition of dimethyl carbonate in normal and inverse ethylene diffusion flames: Nanostructural evidence," *Journal of Environmental Sciences,* vol. 72, pp. 107-117, 2018.

[30] I. Schifter, U. González, and C. González-Macías, "Effects of ethanol, ethyl- tert -butyl ether and dimethyl-carbonate blends with gasoline on SI engine," *Fuel,* vol. 183, pp. 253-261, 2016.

[31] E. G. S. D.Gopinath, "Experimental Investigation on The Effect Adding Di-Methyl Carbonate to Gasoline in a SI Engine Performance," *Scientific and Engineering Research,* vol. 3, no. 6, pp. 92-96, 2012.

[32] M. Bogarra-Macias, J. M. M. Herreros-Arellano, A. Tsolakis, A. P. E. York, and P. Millington, "Reformate Exhaust Gas Recirculation (REGR) Effect on Particulate Matter (PM), Soot Oxidation and Three Way Catalyst (TWC) Performance in Gasoline Direct Injection (GDI) Engines," *SAE International Journal of Engines,* vol. 9, no. 1, pp. 305-314, 2015.

[33] H. J. Seong and A. L. Boehman, "Evaluation of Raman Parameters Using Visible Raman Microscopy for Soot Oxidative Reactivity," *Energy & Fuels,* vol. 27, no. 3, pp. 1613-1624, 2013.

[34] M. Bogarra, J. M. Herreros, A. Tsolakis, A. P. E. York, P. J. Millington, and F. J. Martos, "Impact of exhaust gas fuel reforming and exhaust gas recirculation on particulate matter morphology in Gasoline Direct Injection Engine," *Journal of Aerosol Science,* vol. 103, pp. 1-14, 2017.

[35] K. Kondo, T. Aizawa, S. Kook, and L. Pickett, "Uncertainty in Sampling and TEM Analysis of Soot Particles in Diesel Spray Flame," *SAE Technical Paper 2013-01-0908,* no. 2013-01-0908, 2013.

[36] C. M. Megaridis and R. A. Dobbins, "Morphological Description of Flame-Generated Materials," *Combustion Science and Technology,* vol. 71, no. 1-3, pp. 95-109, 1990.

[37] M. Wozniak, F. R. A. Onofri, S. Barbosa, J. Yon, and J. Mroczka, "Comparison of methods to derive morphological parameters of multi-fractal samples of particle aggregates from TEM images," *Journal of Aerosol Science,* vol. 47, pp. 12-26, 2012.

[38] M. K. Balki and C. Sayin, "The effect of compression ratio on the performance, emissions and combustion of an SI (spark ignition) engine fueled with pure ethanol, methanol and unleaded gasoline," *Energy,* vol. 71, pp. 194-201, 2014.

[39] A. Elfasakhany, "Performance and emissions analysis on using acetone–gasoline fuel blends in spark-ignition engine," *Engineering Science and Technology, an International Journal,* vol. 19, no. 3, pp. 1224-1232, 2016.

[40] J. B. Heywood, *Internal combustion engine fundamentals*. New York: McGraw-Hill, 1988, p. 930.

[41] D. Turner, H. Xu, R. F. Cracknell, V. Natarajan, and X. Chen, "Combustion performance of bio-ethanol at various blend ratios in a gasoline direct injection engine," *Fuel,* vol. 90, no. 5, pp. 1999-2006, 2011.

[42] B. M. Masum, H. H. Masjuki, M. A. Kalam, I. M. Rizwanul Fattah, S. M. Palash, and M. J. Abedin, "Effect of ethanol–gasoline blend on NOx emission in SI engine," *Renewable and Sustainable Energy Reviews,* vol. 24, pp. 209-222, 2013.

[43] M. Abián, S. L. Silva, Á. Millera, R. Bilbao, and M. U. Alzueta, "Effect of operating conditions on NO reduction by acetylene–ethanol mixtures," *Fuel Processing Technology,* vol. 91, no. 10, pp. 1204-1211, 2010.

[44] D. Fennell, J. Herreros, and A. Tsolakis, "Improving gasoline direct injection (GDI) engine efficiency and emissions with hydrogen from exhaust gas fuel reforming," *International Journal of Hydrogen Energy,* vol. 39, no. 10, pp. 5153-5162, 2014.

[45] C. Esarte, M. Abián, Á. Millera, R. Bilbao, and M. U. Alzueta, "Gas and soot products formed in the pyrolysis of acetylene mixed with methanol, ethanol, isopropanol or n-butanol," *Energy,* vol. 43, no. 1, pp. 37-46, 2012.

[46] R. Zhu, J. Hu, X. Bao, L. He, and L. Zu, "Effects of aromatics, olefins and distillation temperatures (T50 & T90) on particle mass and number emissions from gasoline direct injection (GDI) vehicles," *Energy Policy,* vol. 101, pp. 185-193, 2017.

[47] W. Sun, B. Yang, N. Hansen, and K. Moshammer, "The influence of dimethoxy methane (DMM)/dimethyl carbonate (DMC) addition on a premixed ethane/oxygen/argon flame," *Proceedings of the Combustion Institute,* vol. 36, no. 1, pp. 449-457, 2017.

[48] C. Wang, H. Xu, J. M. Herreros, T. Lattimore, and S. Shuai, "Fuel Effect on Particulate Matter Composition and Soot Oxidation in a Direct-Injection Spark Ignition (DISI) Engine," *Energy & Fuels,* vol. 28, no. 3, pp. 2003-2012, 2014.

[49] Y. Luo, L. Zhu, J. Fang, Z. Zhuang, C. Guan, C. Xia, X. Xie, and Z. Huang, "Size distribution, chemical composition and oxidation reactivity of particulate matter from gasoline direct injection (GDI) engine fueled with ethanol-gasoline fuel," *Applied Thermal Engineering,* vol. 89, pp. 647-655, 2015.

[50] N. Serhan, A. Tsolakis, and F. J. Martos, "Effect of propylene glycol ether fuelling on the different physico-chemical properties of the emitted particulate matters: Implications of the soot reactivity," *Fuel,* vol. 219, pp. 1-11, 2018.

[51] C. Hergueta, M. Bogarra, A. Tsolakis, K. Essa, and J. M. Herreros, "Butanol-gasoline blend and exhaust gas recirculation, impact on GDI engine emissions," *Fuel,* vol. 208, pp. 662-672, 2017.

[52] S. J. Harris and M. M. Maricq, "Signature size distributions for diesel and gasoline engine exhaust particulate matter," *Journal of Aerosol Science,* vol. 32, no. 6, pp. 749-764, 2001.

[53] J. Zhu, K. O. Lee, A. Yozgatligil, and M. Y. Choi, "Effects of engine operating conditions on morphology, microstructure, and fractal geometry of light-duty diesel engine particulates," *Proceedings of the Combustion Institute,* vol. 30, no. 2, pp. 2781-2789, 2005.

[54] K. Park, D. B. Kittelson, and P. H. McMurry, "Structural Properties of Diesel Exhaust Particles Measured by Transmission Electron Microscopy (TEM): Relationships to Particle Mass and Mobility," *Aerosol Science and Technology,* vol. 38, no. 9, pp. 881-889, 2004.

[55] K. O. Lee, R. Cole, R. Sekar, M. Y. Choi, J. Zhu, J. Kang, and C. Bae, "Detailed characterization of morphology and dimensions of diesel particulates via thermophoretic sampling," *SAE Technical Paper 2001-01-3572,* 2001.

[56] K. Yehliu, O. Armas, R. L. Vander Wal, and A. L. Boehman, "Impact of engine operating modes and combustion phasing on the reactivity of diesel soot," *Combustion and Flame,* vol. 160, no. 3, pp. 682-691, 2013.

[57] T. Gruber, T. W. Zerda, and M. Gerspacher, "Raman Studies of Heat-Treated Carbon-Blacks," *Carbon,* vol. 32, no. 7, pp. 1377-1382, 1994.

[58] M. Bogarra, J. M. Herreros, A. Tsolakis, A. P. E. York, P. J. Millington, and F. J. Martos, "Influence of on-board produced hydrogen and three way catalyst on soot nanostructure in Gasoline Direct Injection engines," *Carbon,* vol. 120, pp. 326-336, 2017.

[59] M. Lapuerta, F. Oliva, J. R. Agudelo, and A. L. Boehman, "Effect of fuel on the soot nanostructure and consequences on loading and regeneration of diesel particulate filters," *Combustion and Flame,* vol. 159, no. 2, pp. 844-853, 2012.

[60] R. L. V. Wal, "Initial investigation of effects of fuel oxygenation on nanostructure of soot from a direct-injection diesel engine," *Energy & Fuels,* vol. 20, no. 6, pp. 2364-2369, 2006.

[61] R. L. Vander Wal and A. J. Tomasek, "Soot oxidation: dependence upon initial nanostructure," *Combustion and Flame,* vol. 134, no. 1-2, pp. 1-9, 2003.

[62] Y. Zhang and A. L. Boehman, "Oxidation behavior of soot generated from the combustion of methyl 2-butenoate in a co-flow diffusion flame," *Combustion and Flame,* vol. 160, no. 1, pp. 112-119, 2013.

Nomenclature and Abbreviations

a	Exponential factor for particle overlap
A	Area of agglomerate as projected in the micrograph
A_p	Area of the primary particle considered as a circle
BSFC	Brake Specific Fuel Consumption
BTE	Brake Thermal Efficiency
bTWC	before Three-Way Catalyst
C/H	Carbon to Hydrogen Ratio
CAN	Controller Area Network
CO	Carbon Monoxide
CO_2	Carbon Dioxide
COV_{IMEP}	Coefficient of Indicated Mean Effective Pressure
CPC	Condensation Particle Counter
D8	8 % v/v DMC-gasoline fuel blend
DAQ	Data Acquisition
D_f	Fractal Dimension
DMA	Differential Mobility Analyser
DMC	Di-Methyl Carbonate
dp_0	Primary Particle Diameter
EGR	Exhaust gas recirculation
ETBE	Ethyl Ter-Butyl Ether
EVC	Exhaust Valves Closing
F_t	Fringe Tortuosity
FTIR	Fourier Transform Infrared
GDI	Gasoline Direct Injection
GNMD	Geometry Number Mean Diameter
GPF	Gasoline Particulate Filter
HC	Unburnt Hydrocarbons
HCCO	Ketenyl Radicals
HEPA	High Efficiency Particle Arrestance
IMEP	Indicated mean effective pressure
IVO	Intake Valves Opening
K_f	Pre-factor or structural coefficient
L	Length of rectangle containing the minimum area
L_a	Fringe Length
LHV	Lower Heating Value
M	Number of pixels per agglomerate
MBT	Maximum Brake Torque
MFB	Mass Fraction Burnt
MMLRT	Maximum Mass Loss Rate Temperature
MTBE	Methyl Ter-Butyl Ether
n	Number of Primary Particles per Agglomerate
NEDC	New European Driving Cycle
NO	Nitric Oxide
NO_x	Nitrogen Oxides
O/C	Oxygen to Carbon Ratio
PFI	Port Fuel Injection
PM	Particulate Matter
Pmax	Maximum in-cylinder pressure
PSD	Particle Size Diameter
RAMAN	Raman Spectroscopy

RFF	Roof Factor Form
r_i	Distance between the centre of a primary particle and the centroid of the agglomerate
R_g	Radius of Gyration
SI	Spark Ignition
SMPS	Scanning Mobility Particle Sizer
SPSS	Statistical Package for Social Science
SSA	Surface area/volume ratio
TDC	Top Dead Centre
TEM	Transmission Electron Microscope
TGA	Thermogravimetric Analysis
THC	Total unburnt Hydrocarbons
TWC	Three-Way Catalyst
VOMs	Volatile Organic Materials
W	Width of rectangle containing the minimum area

List of figures

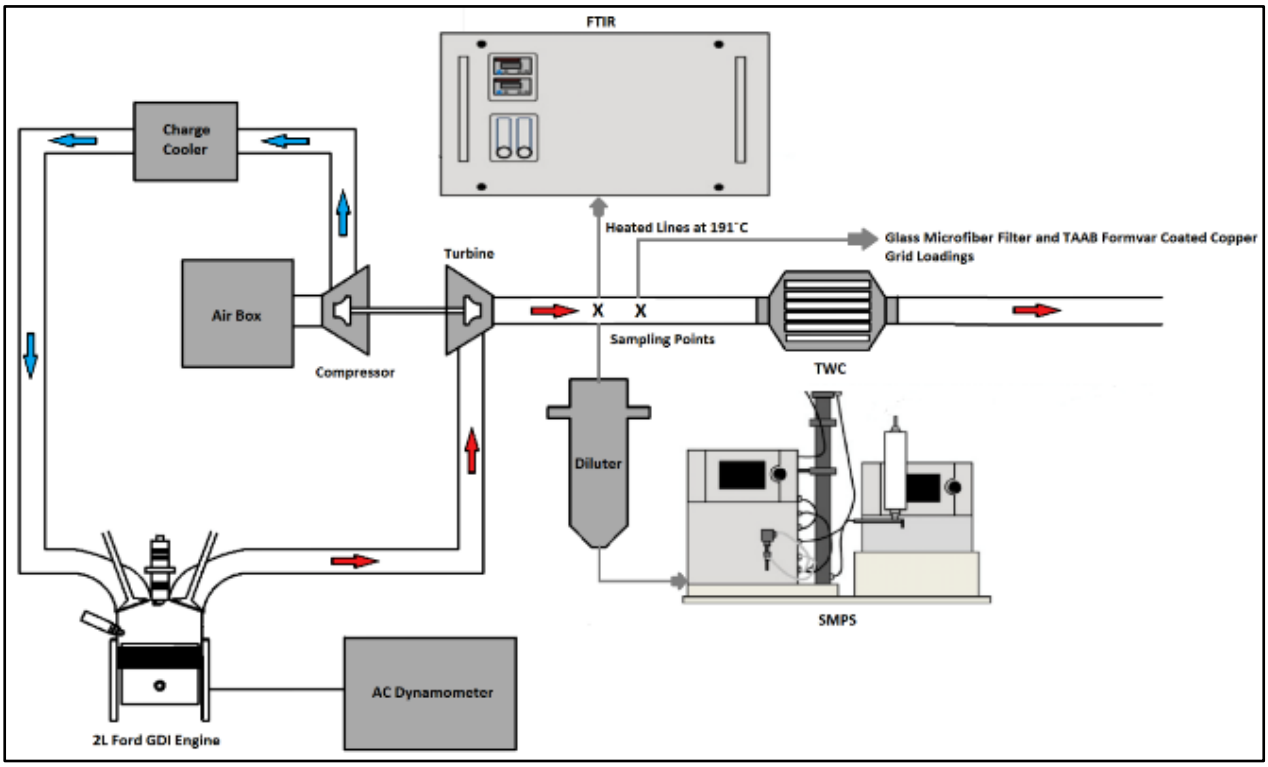

Figure 1: Schematic Drawing of Experimental Setup

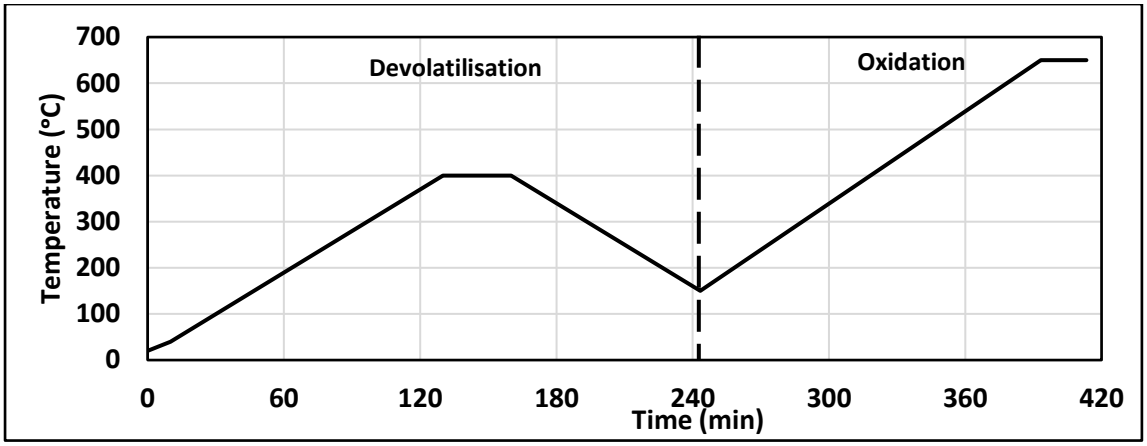

Figure 2: TGA Temperature Ramp Program

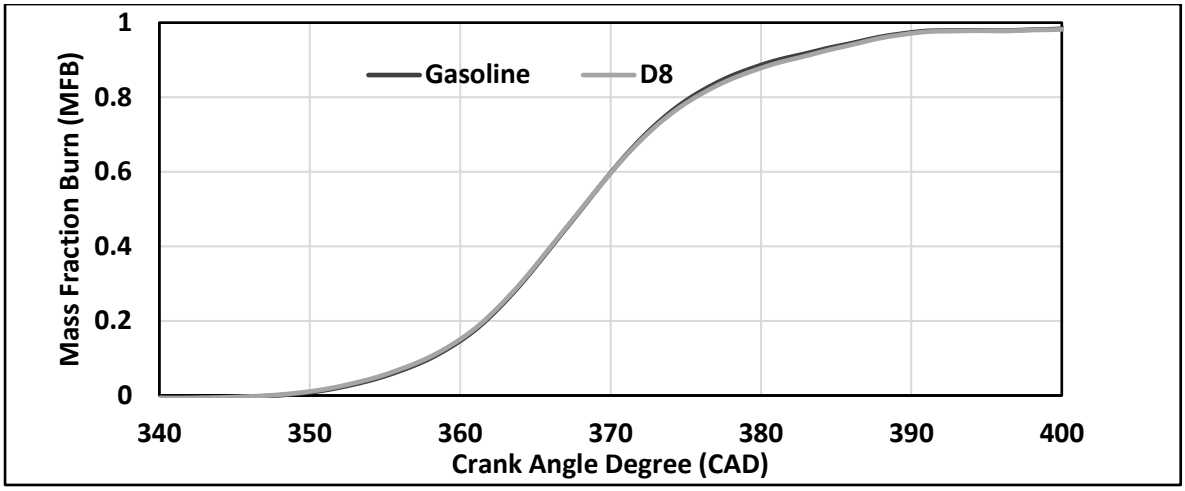

Figure 3: MFB plot for Gasoline and D8.

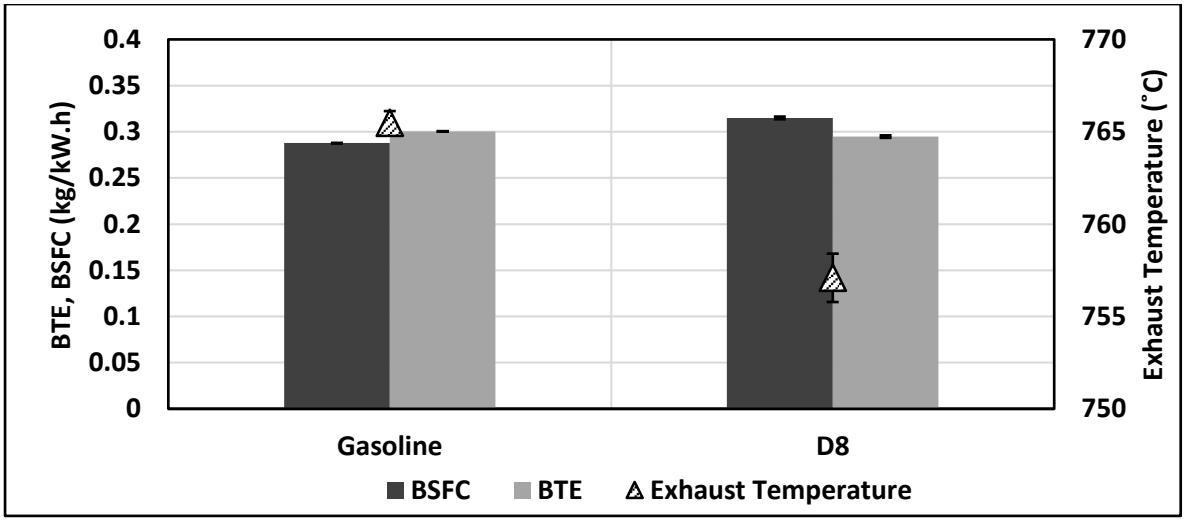

Figure 4: Exhaust Gas Temperature, Brake Thermal Efficiency and Equivalent Brake Specific Fuel Consumption

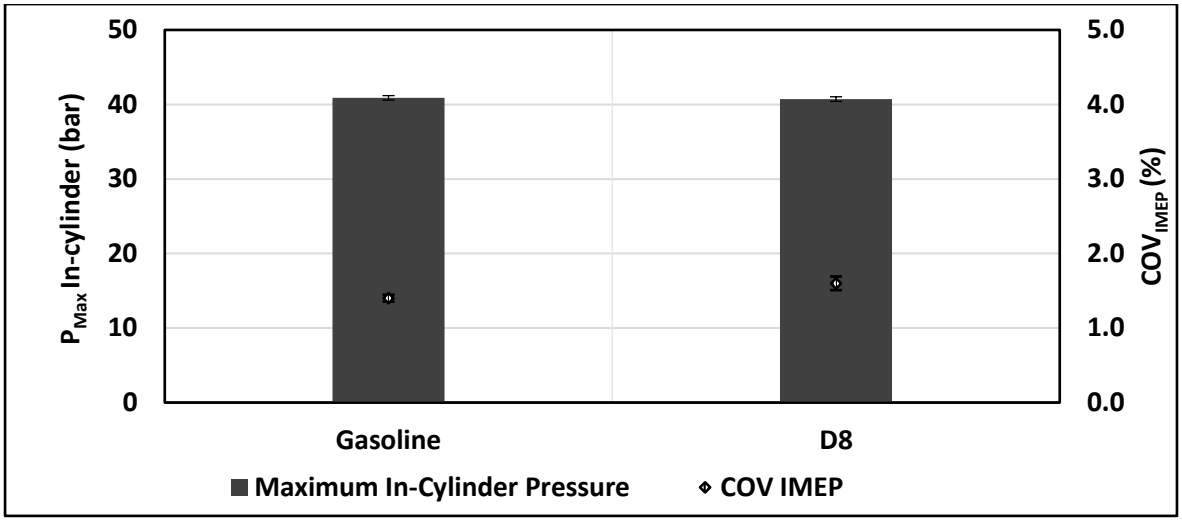

Figure 5: Maximum In-Cylinder Pressure and COV of IMEP

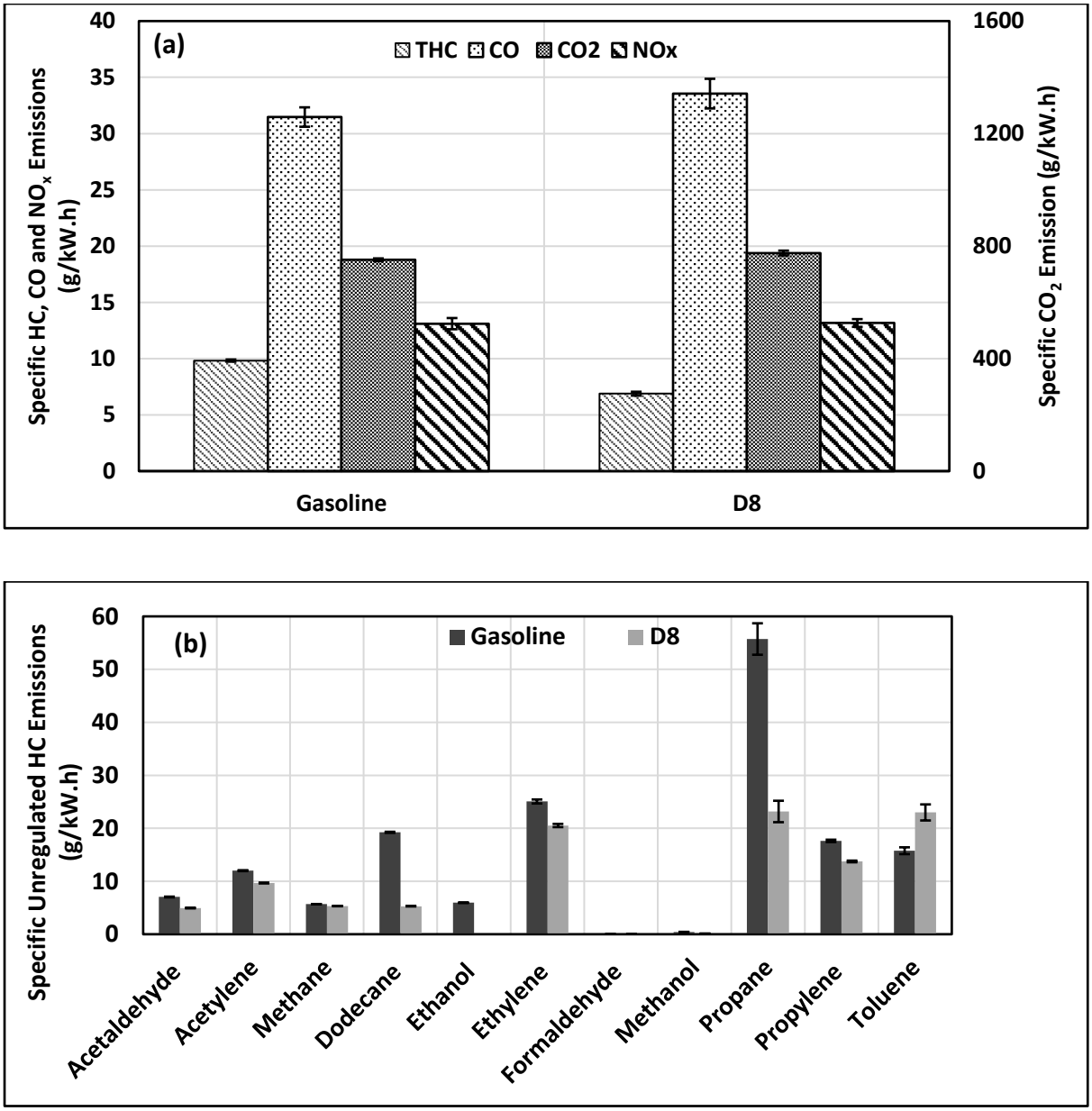

Figure 6: (a) Specific gaseous **(b)** HC species emissions for gasoline and D8

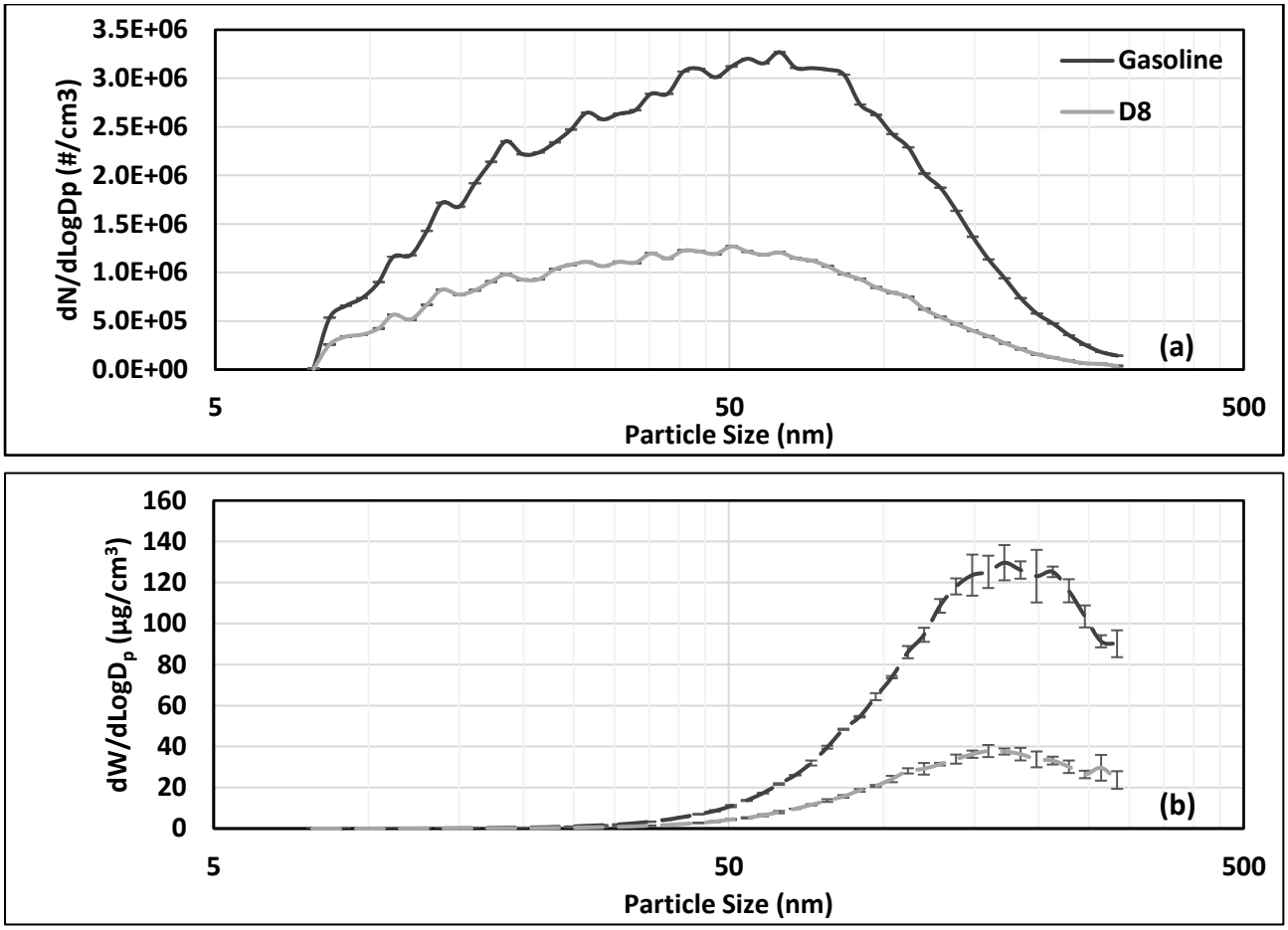

Figure 7: Particle Size Distribution by **(a)** Number **(b)** Mass emitted by gasoline and D8

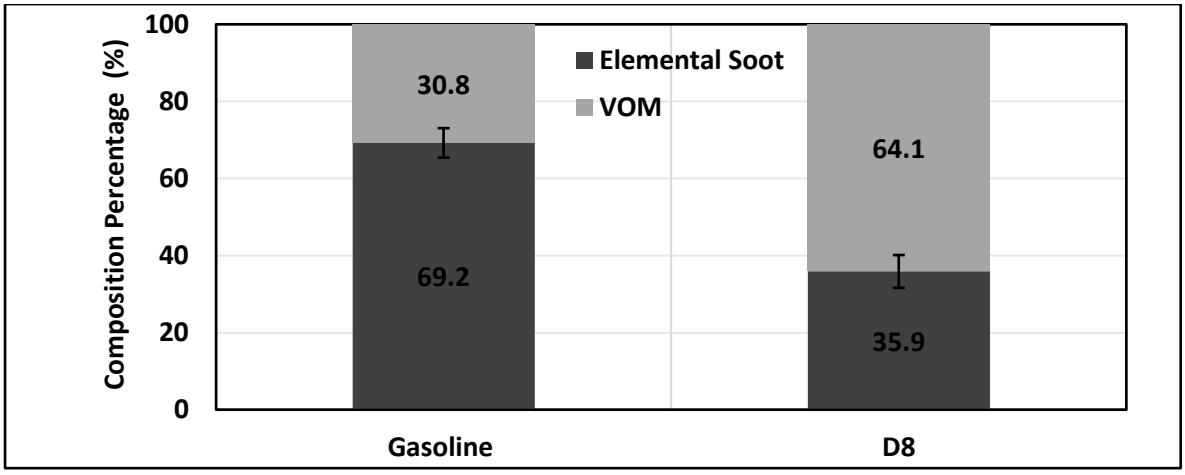

Figure 8: PM Compositions for gasoline and D8

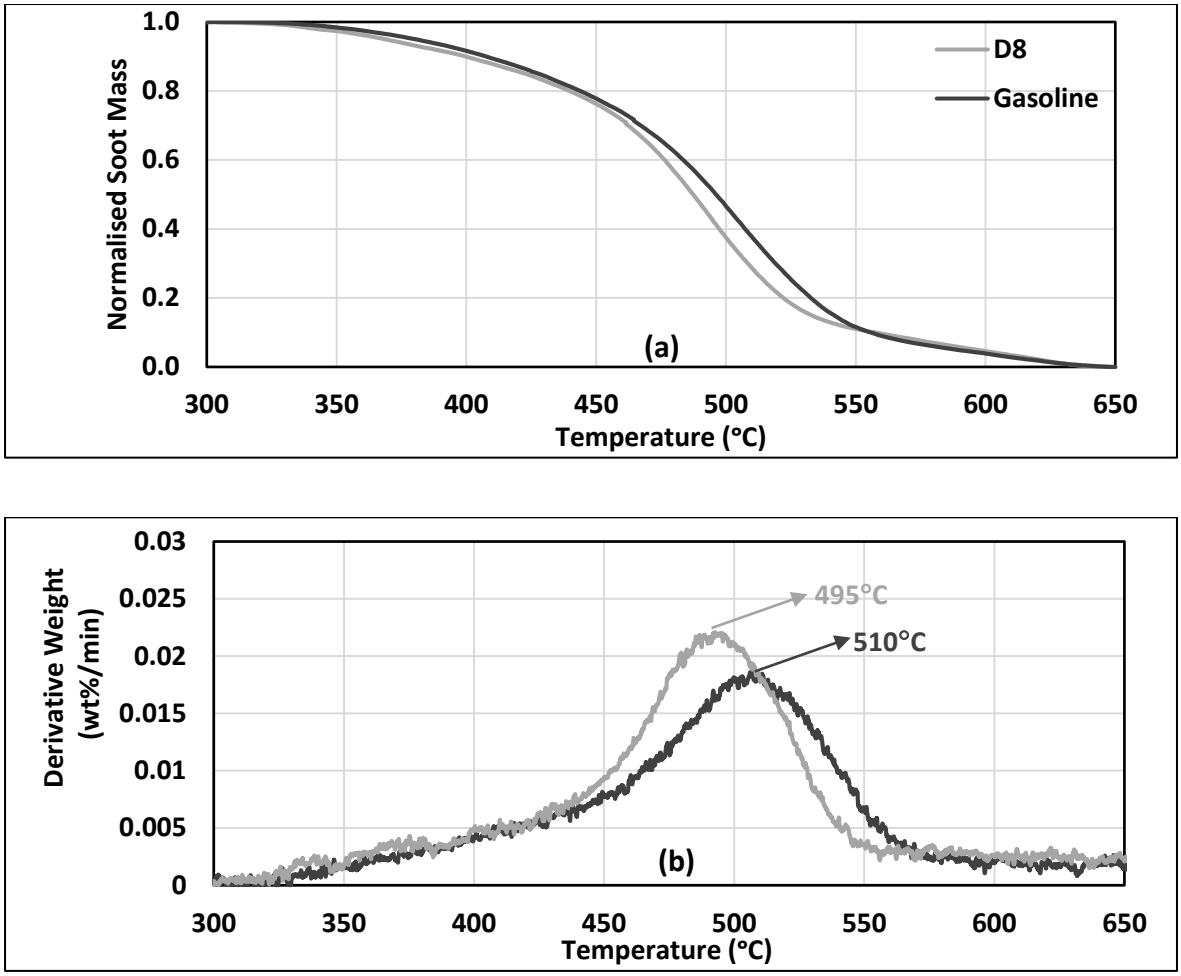

Figure 9: (a) Soot Oxidation Mass Profile **(b)** Maximum Mass Loss Rate Temperature for soot emitted by gasoline and D8

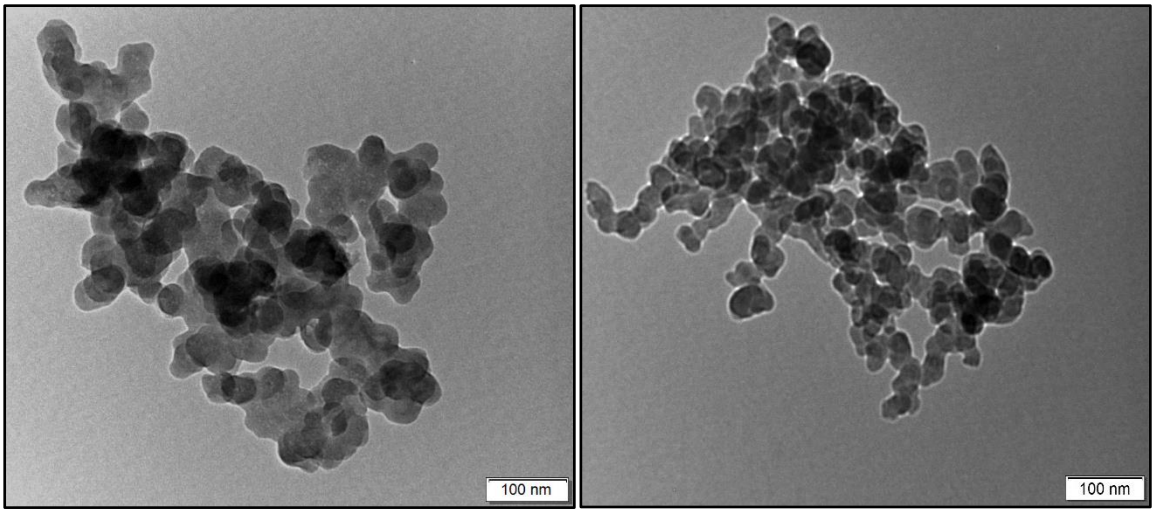

Figure 10: TEM Micrographs of PM agglomerate for gasoline (*left*) and D8 (*right*) at 80k magnification

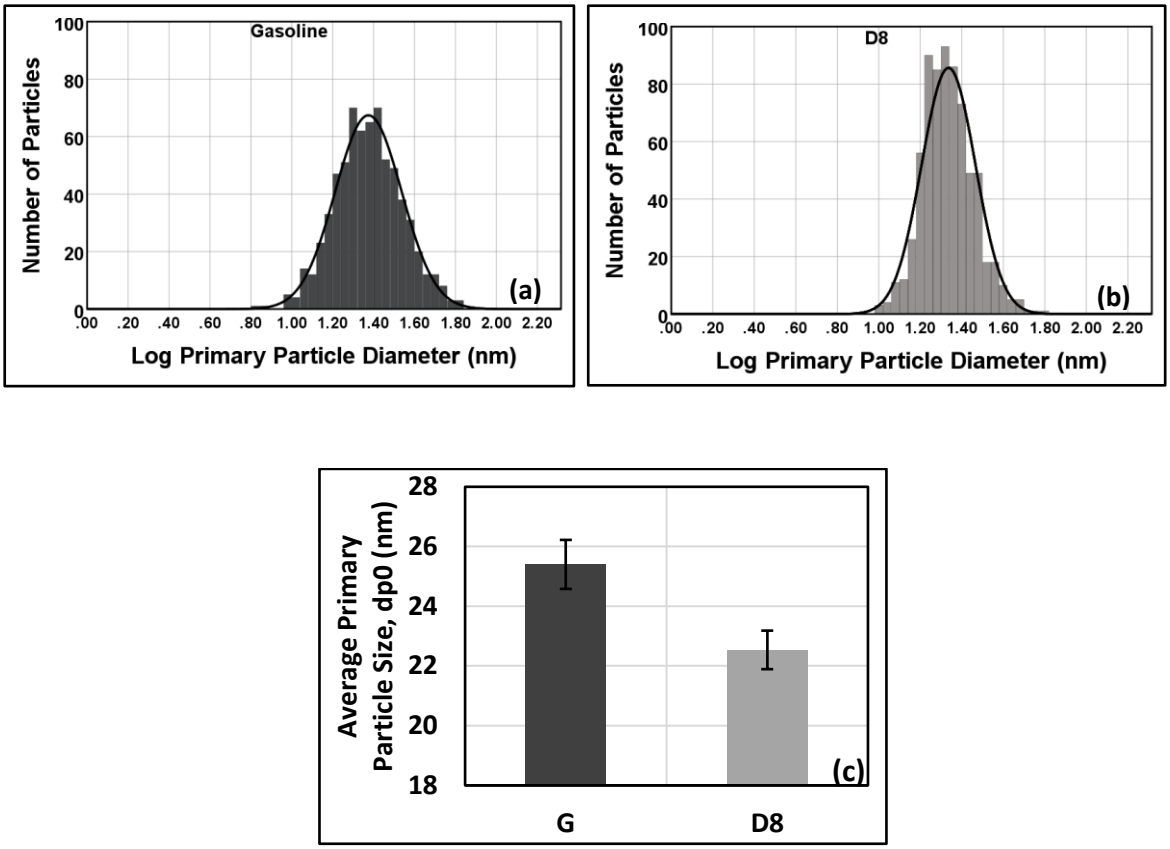

Figure 11: Primary Particle Distribution for **(a)** gasoline (G), **(b)** D8 and **(c)** Average Primary Particle Size

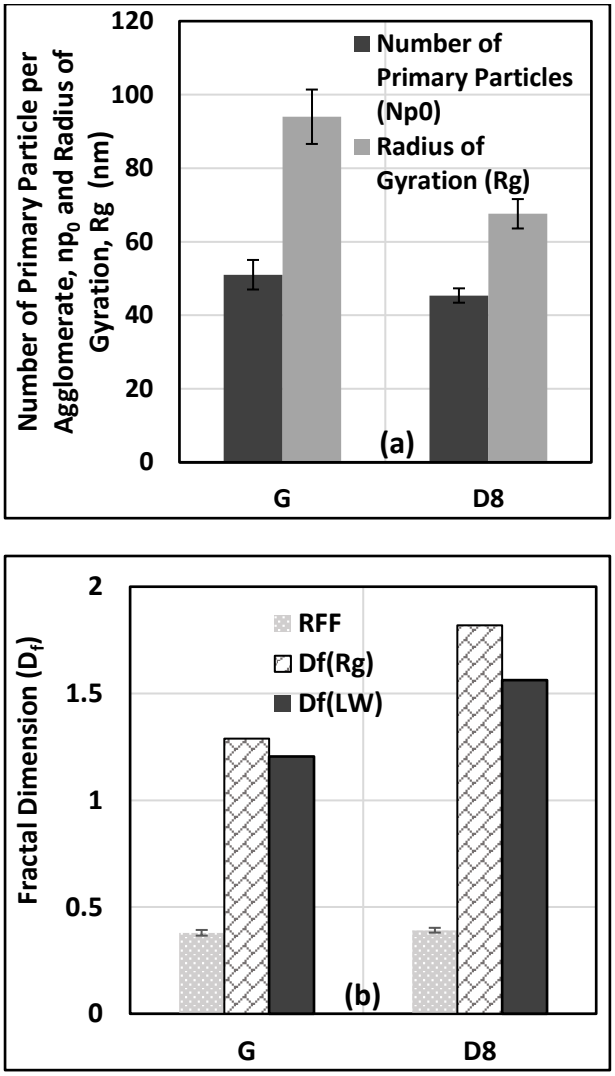

Figure 12: (a) Number of Primary Particles per Agglomerate and Radius of Gyration **(b)** Fractal Dimension

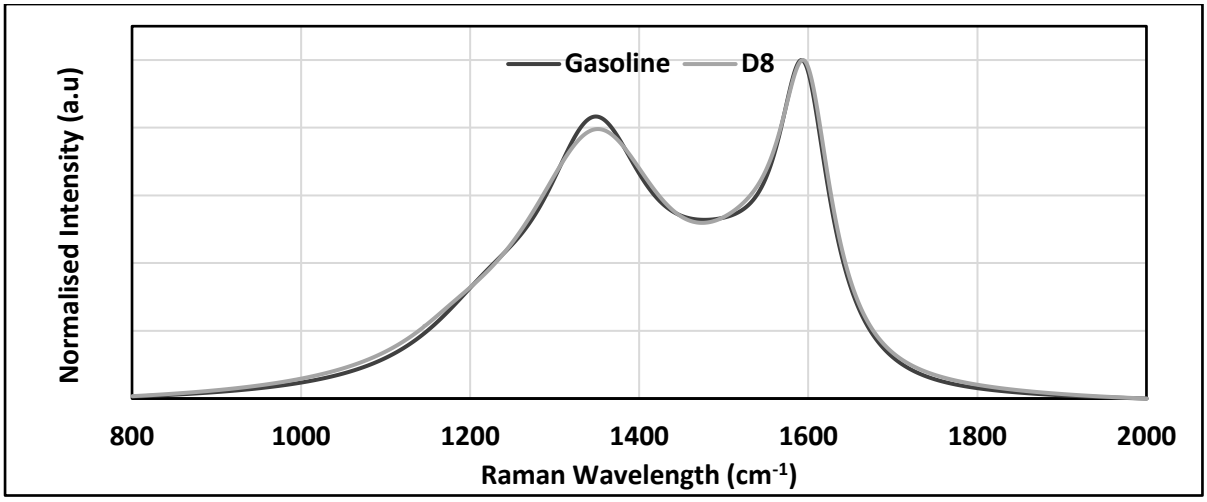

Figure 13: Average Raman Spectra

List of tables

Table 1: Engine Specification

Engine Specification	
Compression Ratio	10:1
Bore x Stroke	87.5 x 83.1 mm
Turbocharger	Borg Warner k03 with variable wastegate
Rated Power	149 kW at 6000 rpm
Rated Torque	300 N.m at 1750-4500 rpm
Engine Management	Bosch ME17
Number of Cylinders	4
Firing Order	1-2-4-3
Fuel Injection System	Direct Injection (DI)

Table 2: Fuels Properties

	Gasoline	**DMC**	**D8**
Chemical Formula	$C_{5.18}$ $H_{9.94}$ $O_{0.16}$	$C_3 H_6 O_3$	$C_{5.05}$ $H_{9.72}$ $O_{0.44}$
Octane Number (RON)	96.8*	101-120	97.2-98.7
Lower Heating Value (MJ/kg)	41.65*	15.78	38.8
Vapour Pressure @ 20 ˚C (kPa)	59.8-65.9*	5.3	-
Kinematic Viscosity @ 40°C (mm^2/s)	~0.8	~0.6	-
Heat of Vaporization (kJ/kg)	350	~400	~355
Laminar Flame Velocity @ 1 bar, 325K (cm/s)	33	~36	-
Initial Boiling Point (˚C)	35.5*	41.9	-
Final Boiling Point (˚C)	199.2*	203.7	-
O (mass %)	3.48*	53.28	9.09
Density @ 15°C (g/cm^3)	0.7466*	1.076	0.7730
Air Fuel Ratio @ Stoichiometric	14.22	9.15	13.66

* Shell Analyses Report, ~ approximate value

Table 3: Experimental Matrix of Engine Bench Test

Stoichiometry		λ=1
Speed (rpm)		2200
Torque/Load (N.m)		90
Intake Valves Opening (CAD aTDC)		11
Exhaust Valves Closing (CAD aTDC)		8
Injection Timing (CAD bTDC)		300
Spark Timing (CAD bTDC)	**Gasoline**	27
	D8	26

Table 4: TGA Methodology

Step	Temperature	Flows
1	**Hold for 10 minutes at 40 ˚C**	Purge: N_2 60ml/min, Sheath: N_2 40 ml/min
2	**Heat up to 400 ˚C at 3 ˚C/min**	
3	**Hold for 30 minutes at 400 ˚C**	
4	**Cool down to 150 ˚C at 3 ˚C/min**	
6	**Heat up to 650 ˚C at 3 ˚C/min**	Purge: N_2 60ml/min, Sheath: Air 40 ml/min
7	**Hold for 30 minutes at 650 ˚C**	
8	**Cool down to 40 ˚C at 50 ˚C/min**	

Table 5: Statistical Normality Tests

Null Hypothesis	Significance	Results
The distribution of Log(Gasoline) is normal with mean 1.37 and standard deviation 0.162	0.200[a]	Retain null hypothesis
The distribution of Log(D8) is normal with mean 1.34 and standard deviation 0.130	0.131[a]	Retain null hypothesis
Asymptotic significances are displayed. The significance level is 0.05		

[a] Lilliefors corrected

Table 6: I_{D1}/I_G, A_{D1}/A_G, I_{D3}/I_G, A_{D3}/A_G and L_a obtained from Raman spectra for gasoline and D8.

Fuel	**I_{D1}/I_G**	**A_{D1}/A_G**	**D1 FWMH**	**I_{D3}/I_G**	**A_{D3}/A_G**	**L_a**
Gasoline	0.94 ± 0.10	2.01 ± 0.38	152 ± 10	0.35 ± 0.02	0.49 ± 0.04	2.25 ± 0.40
D8	1.05 ±0.06	2.99 ± 0.42	205 ± 25	0.38 ±0.01	0.73 ± 0.02	1.50 ± 0.20